JOURNAL OF THERMOPHYSICS AND HEAT TRANSFER
Vol. 11, No. 1, January–March 1997

Evaluation of Real-Gas Phenomena in High-Enthalpy Impulse Test Facilities: A Review

Chul Park*
Tohoku University, Aramaki, Aoba-ku, Sendai 980-77, Japan

The feasibility of experimentally evaluating the high-temperature real-gas effects on the fluid–mechanical behavior of hypersonic flows in shock tunnels and hot-shot tunnels is examined. Considering the intrinsic limitations of those facilities, the real-gas effects on aerodynamic characteristics, separated flows, and shock-boundary-layer interactions, turbulent transitions, and leeward/base flow are considered to be the possible subjects of simulation in those facilities. A new empirical reaction rate model is proposed to numerically reproduce the existing experimental data on species concentrations. Based on this model, the average density ratios expected across a normal shock wave formed over a model placed in an impulse tunnel are calculated. By comparing these density ratios with the flight values, it is pointed out that the best simulation is achievable at an enthalpy of 8 MJ/kg, and that two-thirds of the real-gas effects could be simulated at that enthalpy. It is proposed that the real-gas effects measurements in an impulse tunnel be validated by comparing the flow patterns over simple shapes obtained in a tunnel with those obtained in a ballistic range.

Introduction

DURING the past cold-war era, many types of launch vehicles and re-entry vehicles were developed by various nations, primarily for the purpose of ensuring their military security. The ending of the cold-war and the strong emergence of the commercial use of communications satellites are shifting the emphasis into providing an inexpensive and reliable launch system. A large number of commercial satellites are presently envisioned to be launched in the near future. The worldwide competition to capture this new market is strong. To meet this challenge, a new class of economical reusable launch systems is being developed by various nations.

To design such an efficient aerospace vehicle, forces and moments and wall heat transfer rates on the surface of the vehicle must be known accurately. To experimentally verify the accuracy of those design parameters, wind-tunnel tests are needed. To produce flows of desired temperatures, Mach numbers, and Reynolds numbers in the test section at a hypersonic flight speed, such tunnels must be operated at very high enthalpies and reservoir pressures. There are no materials that can withstand such temperatures and pressures in a steady state. Only impulse tunnels, which operate for a few milliseconds, could function at those conditions. Two types of impulse tunnels exist: 1) shock tunnels and 2) hot-shot tunnels. In shock tunnels, the high-temperature, high-pressure gas in the reservoir is produced by shock-heating a stationary gas using the shock-tube technique. The driver gas for this operation is prepared either by heating the container, combustion or detonation, or piston compression. In hot-shot tunnels, the test gas is heated by an impulsive electric discharge in the reservoir.

In addition to Mach numbers and Reynolds numbers, hypersonic test facilities must simulate the high-temperature real-gas phenomena. At an enthalpy of about 3 MJ/kg or higher, air molecules become vibrationally excited, dissociated, and ionized behind a shock wave. These high-temperature real-gas phenomena absorb heat, and as a result, the effective γ decreases and compressibility increases. These phenomena cause changes in pressure distribution, and thereby aerodynamic characteristics of the vehicle and its components. At the wall surface the dissociated and ionized species recombine and produce heat.

In the reservoir of such an impulse tunnel, the test gas is at a high temperature, and therefore, is in a significantly vibrationally excited, dissociated, or ionized state. During the cooling process occurring in the nozzle, vibrational de-excitation and recombination processes move the gas state toward that of the natural atmosphere. However, these processes require time to complete, and since the temperature of the test gas changes so rapidly in the nozzle, the gas fails to reach the chemical equilibrium condition of the natural atmosphere at the nozzle exit. This phenomenon is known as chemical freezing. It is undesirable because the real-gas effects of concern may not be simulated faithfully in such a flow.

The ratio between the characteristic flow residence time and the time required for completion of chemical reactions, which is a measure of the extent of chemical nonequilibrium, is known as the Damköhler number. The atomic recombination processes occurring in the nozzle are three-body processes, and, therefore, their rates are proportional to the square of gas density ρ. The gas residence time in a nozzle is proportional to the length of the nozzle L. Therefore, the Damköhler number in the nozzle is proportional to $\rho^2 L$. Theoretically, the freezing phenomenon could be prevented by making the gas pressure in the nozzle very high and the nozzle very long. For this reason, large impulse tunnels have recently been constructed worldwide. Such tunnels can produce reservoir pressures of up to 200 MPa, and have a nozzle length of several meters.

Questions exist as to what extent those facilities succeed in preventing chemical freezing, to what extent the freezing phenomenon can be tolerated, and what is the most appropriate use of those facilities. It is the purpose of this paper to answer these questions. By reviewing recent experimental data, this paper attempts to do the following:

1) Identify the types of real-gas effects that could realistically be simulated.

2) Develop an empirical reaction rate model that numerically reproduces the experimentally obtained species concentration data.

Received May 17, 1996; presented as Paper 96-2234 at the AIAA 27th Fluid Dynamics Conference, New Orleans, LA, June 17–20, 1996; revision received Sept. 18, 1996; accepted for publication Sept. 19, 1996.

*Professor, Department of Aeronautics and Space Engineering. Associate Fellow AIAA.

3) Find the most appropriate regimes of operation and validation method for the tests made in those facilities.

Requirements

In Ref. 1 the external flow phenomena influenced significantly by the high-temperature real-gas phenomena are classified into seven types. They are 1) aerodynamic characteristics, 2) separated flows and shock-boundary-layer interactions, 3) boundary-layer transitions, 4) leeward-side/base flows, 5) radiation and ablation, 6) ionization and radio blackout phenomenon, and 7) gas-surface interactions. These problems are shown schematically in Fig. 1. These are the flow problems that the real-gas laboratory facilities are expected to simulate:

1) The influence of real-gas effects on aerodynamic characteristics is well known. The heat absorption by chemical reactions behind a shock wave causes a decrease in the effective γ, and thereby increases the average density ratio between the shock layer and the freestream. To satisfy the mass continuity condition, the shock-layer thickness decreases inversely with the density ratio. This lowers the angle of the shock wave formed over an inclined surface, which leads to a lower lift and drag and a positive (nose-up) pitching moment. Such phenomena have been observed in both Apollo and Space Shuttle flights.[2,3] To test this phenomenon in an impulse tunnel, the average density ratio across a shock wave formed in the test section must be the same as that occurring in flight.

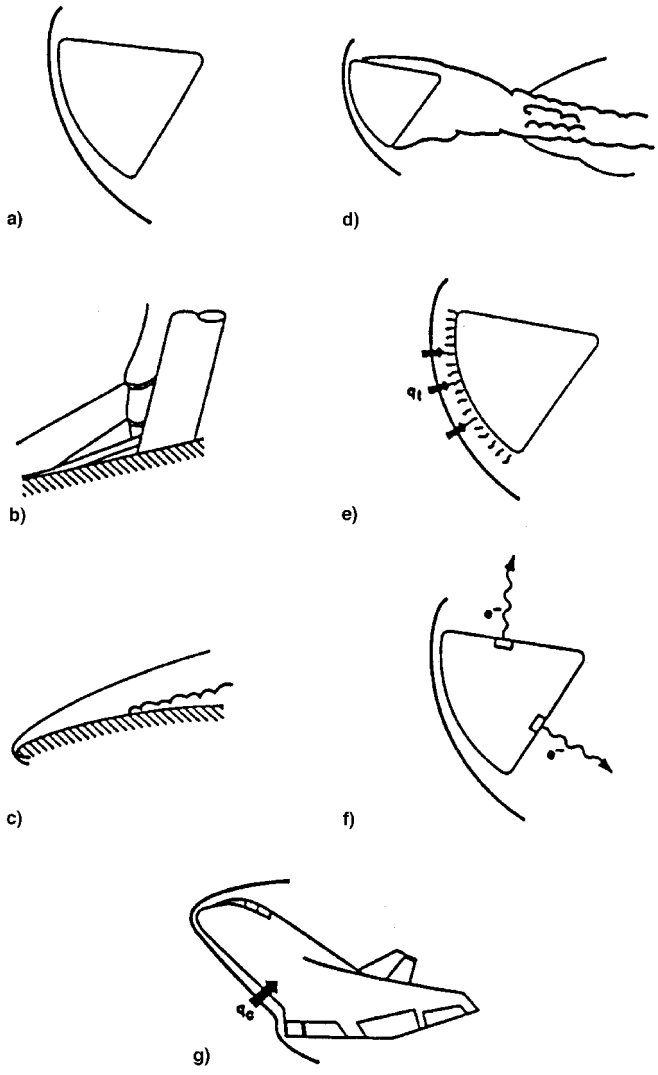

Fig. 1 Classification of high-temperature real-gas problems[1]: a) aerodynamic characteristics, b) separated and/or shock-/boundary-layer interactions, c) turbulent transition, d) leeward side/base flows, e) radiation and ablation, f) radio blackout, and g) gas-surface interactions.

2) Flow separation phenomenon occurs over the compression corners generated by deflected control surfaces, in decelerating flows such as those in the inlet of scramjet engines, and in shock-on-shock or shock-on-boundary-layer interactions. The separated region in those flows tends to shrink in the real-gas regime because of the heat absorption by dissociation therein. This leads to an improvement in the effectiveness of the control surfaces.[4] Likewise, flow separation in a decelerating flow is likely to be either suppressed, delayed, or its extent reduced by the chemical reactions. To simulate these phenomena in a laboratory, both the extent of heat absorption and the associated Damköhler number must be reproduced. These flowfields are affected also by the level of turbulence, and so, in addition, the turbulence level must be simulated.

3) The data obtained from the flight of the Space Shuttle vehicle indicated that the laminar-to-turbulent transition occurred at Reynolds numbers higher than in a perfect-gas flow.[5] A boundary layer is known to be stable when the curvature in the density variation across the layer is small. The curvature is smaller in a chemically reacting flow than in a perfect-gas flow because of the heat absorption. To test this phenomenon in a laboratory, the level of turbulence and the chemical behavior involved must be simulated.

4) The dynamics of the flow in the leeward-side or base region are dictated mostly by separation and shear-flow phenomena, which are in turn determined by the level of turbulence in the flow entering the region. The density of the flow in this region is usually low, and, therefore, chemical reactions are mostly frozen. The thermodynamic behavior of the flow can be described by a fixed effective γ, which is determined by the atom mole fractions of the flow entering this flow region. To simulate this flowfield, the turbulence level and the effective γ need to be reproduced.

5) Radio blackout occurs when the gas around a vehicle is ionized. In flight, ionization occurs mostly by the formation of NO^+. In an impulse tunnel, ionization occurs mostly to the metallic impurities. To test this phenomenon, the freestream gas must be completely free of such impurities.

6) Radiative heating becomes a problem at flight enthalpies greater than 50 MJ/kg. Such high enthalpies cannot be produced in an impulse tunnel with present-day technology. To study the ablation phenomenon, the facility must provide a steady flow of long duration, which is not possible with an impulse facility.

7) The gas–surface interaction phenomenon is usually studied in arc-heated wind tunnels because the problem of concern is of a steady-state nature. However, some aspects of the problem, such as determining the difference in heat transfer rates between the catalytic and noncatalytic surfaces, should be possible in an impulse tunnel. Since the gas reaches equilibrium at the boundary-layer edge in most practical problems of interest, only the enthalpy and Reynolds numbers need to be simulated for this purpose.

For the scramjet propulsion system, the flows outside the combustion chamber, i.e., the flows over the inlet and in the nozzle, can be considered to be one of the external flows considered previously. In the supersonic flight speed range, the delay of ignition of the fuel–air mixture is a problem unique to the internal flow. However, in the hypersonic range, ignition is generally fast because the flow entering the combustion chamber is at a high temperature. In flight, the airflow entering the combustion chamber is likely to be turbulent because of the presence of a long inlet. The flow may also contain impurities resulting from the gas injection at or ablation of the heat shield over the nose or cowl lip. In so-called direct connect or semidirect connect tests in an impulse tunnel, the flow entering the combustion chamber correctly simulates these hot, turbulent, and impure flow conditions existing in the flight environment.

However, the flows produced in an impulse facility also contain the dissociated species in the freestream, which could potentially affect the combustion processes. These dissociated species can be removed by providing a compression ramp ahead of the combustion chamber, that is, by adopting a semi-direct connect method. This is because the higher pressure and temperature over the ramp is efficient in promoting equilibration. How close to equilibrium the flow is at the combustion chamber entrance depends on the pressure and dimensions of the facility. Thus, the usefulness of an impulse facility for a scramjet engine test is determined mostly by the scale performance of the facility, i.e., flow Mach number, total pressure, enthalpy, Reynolds number, and flow duration. These issues are outside the scope of the present work. For these reasons only the external flow problems are considered in the present work.

Facility Limitations

The foregoing discussions show that a real-gas facility must produce not only the required Mach numbers, Reynolds numbers, and enthalpies, but also an unexcited and undissociated quiet flow, as well as correct Damköhler numbers. Impulse tunnels can only partly fulfill these requirements because of their intrinsic limitations, which are described next.

Turbulence

All wind tunnels produce acoustic noises in the turbulent boundary layers over the wall of the throat and the nozzle. In a shock tunnel, the diaphragm-opening process and the interaction of the reflected shock at the endwall with the boundary-layer flow, which produces jets and separated flows, produce noise. If the driver gas of a shock tunnel is prepared by piston compression, the pressure waves generated by the moving piston introduce pressure fluctuations in the reservoir. If a combustion or detonation is used to heat the driver gas, noise is produced by those processes. In hot-shot tunnels, the electric discharge produces similar pressure waves. These phenomena, and the ablation phenomena described next, cause an early transition of a boundary layer over the tested models, resulting in an increase in the effective Reynolds number of the freestream flow.

Ablation

The high heat transfer rates over the endwall and the nozzle-entrance regions of a shock tunnel or over the wall of the reservoir of a hot-shot tunnel cause the wall to ablate. The presence of ablated material in the test gas can be verified by observing the spectrum of the radiation emitted by the shock layer formed over a model placed in the test section. An example of such a spectrum[6] is shown in Fig. 2. It shows many metallic species. By observing the intensity of the light emitted by the shock layer in front of each of the pitot heads of a pitot rake placed in the test section, one can determine the radial distribution of those ablation product species. Invariably, the ablation products are seen to be nearly uniformly distributed in the radial direction.

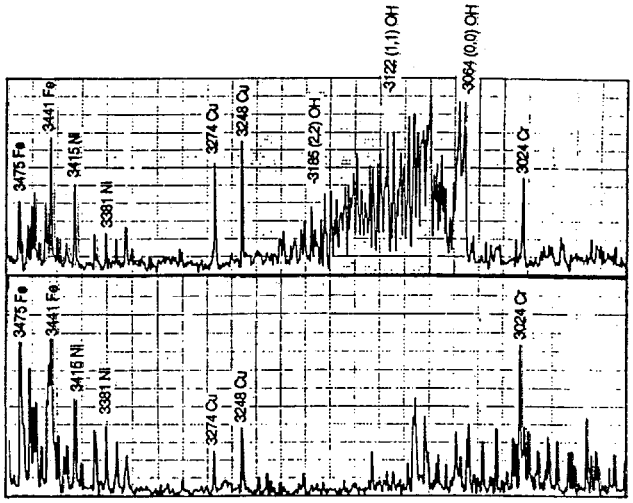

Fig. 2 Radiation spectra emitted from the shock layer over a blunt body placed in a shock tunnel.[6] The top trace: copper nozzle and nitrogen–water vapor as test gas; bottom trace: steel nozzle and air as test gas.

The concentrations of the impurity species can be calculated from the spectrum shown in Fig. 2. The calculated impurity concentration is usually very small. The relative concentration of the metallic impurities can be estimated also by weighing the endwall and nozzle-entrance materials before and after a run. In an experimental program conducted at the NASA Ames Research Center, the mass of the wall material lost in a single run was seen to reach a maximum of 1% of the test gas mass.

The ablation phenomenon accompanies spallation by which solid or liquid particulates are released into the inviscid region of the reservoir.[7] Presumably, the particulates are released with a very low speed. Their presence at the centerline of the test section implies that they migrate outward toward the inviscid region. One suspects that the velocity gradient in the boundary layer causes the particulates to rotate, and the relative velocity between the flow and a rotating particle produces a magnus force that is directed outward. The gaseous ablation products condense in the cooling process in the nozzle, producing a secondary source of particulates in the test section.

Even when an impulse tunnel is operated at relatively low pressures and enthalpies, the flow tends to contain a small amount of metallic impurities. These impurities are believed to be introduced into the test gas through desorption from the wall prior to a run.[8]

To avoid ablation, the wall must be made with a high-conductivity, temperature-resistant material such as molybdenum, and reservoir pressure and enthalpy must be kept below about 100 MPa and 20 MJ/kg, respectively. However, even with these measures, it is unrealistic to hope to completely remove the metallic impurities from the flow.

These species ionize easily, and, therefore, their presence precludes the testing of the radio blackout phenomenon. When they condense on the wall, they change the surface catalycity, and, therefore, the study of the gas–surface interaction problem is hampered.

The ablation products in the test gas changes the energetics of the test gas. However, since their concentrations are still small, the changes in the thermochemistry of the test gas are relatively small.

Enhancement of Damköhler Numbers

In the flow behind a shock wave in which the gas dissociates and ionizes, the reactions are binary, that is, their rates are proportional to density. Therefore, the characteristic Damköhler number is proportional to the product of density and length scale. Since Reynolds numbers are proportional also to the same product, theoretically the needed Damköhler numbers could be automatically simulated when the Reynolds numbers are simulated. However, this argument does not hold for the impulse tunnels. The rates of reactions behind a shock wave over the test model are affected by the chemical state of the freestream flow. A freestream flow containing vibrationally or electronically excited species or dissociated or ionized species produces reaction rates faster than an undisturbed flow. In an experiment conducted in an arcjet wind tunnel, the rate of approach to equilibrium behind a bow shock wave was found to be at least 20 times faster than in an undisturbed flow.[9]

The metallic impurity species mentioned earlier can participate in the rate processes. However, their contribution is probably small compared with those of the O and N atoms, especially in their electronically excited states, and the elec-

tronically excited N_2, O_2, and NO molecules, whose concentrations are much greater. Thus, the presence of a small concentration of impurity species is probably insignificant in this respect.

These considerations lead one to believe that meaningful tests are possible at best only for the problems 1–4 and part of 7, out of the seven listed previously. Even for testing these five problems, a compromise must be made in that 1) a finite level of turbulence and the resulting increase in the effective Reynolds numbers, 2) the changes in the extent of heat absorption behind the shock wave caused by the presence of dissociated species and ablation products in the freestream, and 3) the enhancement in the effective Damköhler numbers caused by the presence of the energetic species in the freestream, must be accepted and compensated for in the data reduction. Such procedures will be described in the Test Strategy section.

Ballistic Ranges

The difficulties just mentioned can be avoided if the model is flown in the test gas instead of the test gas being made to flow over the model. This is done in a ballistic range. The largest ballistic range in existence can launch a model of 8 cm in diameter to a velocity of up to 8 km/s, into a test gas up to an atmospheric pressure.[10] Ballistic ranges can easily reproduce the Reynolds and Damköhler numbers of large hypersonic vehicles.

There are no aerothermodynamic problems in simulating the flowfields 1–4, and possibly 5, mentioned previously in a ballistic range. There has been skepticism in the past[11] that laminar-to-turbulent transition of a boundary layer may not be simulated in a ballistic range because of what is termed the unit Reynolds number effect. The transition data obtained in a ballistic range with sharp cones indicated that transition Reynolds number changes with the model size. This is probably because the tip of the sharp cone ablates, and the extent of ablation changes with freestream density. In practice, the nose tip of all hypersonic objects is blunt. For a blunted cone free of ablation, transition is likely to be consistent, although such tests have not yet been made systematically.

However, there are two basic limitations to the ballistic range. First, ballistic ranges cannot launch a model that produces a significant amount of lift. A lifting model tends to veer away from the centerline of the range test section and hit its sidewalls before data can be gathered. Second, only limited instrumentation is permitted. Because of these two limitations, the ballistic range tests are suitable only for models of relatively simple geometry with small lift, such as spheres and cones, and Apollo-like weakly lifting bodies. Only optical flow visualization is practical, though telemetry is possible at an expense.

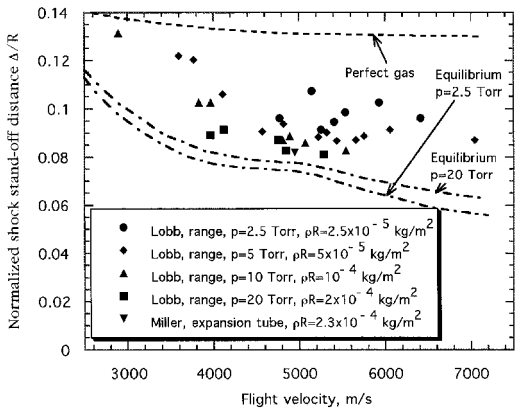

Fig. 3 Shock standoff distance for sphere in nonequilibrium regime.[13,14]

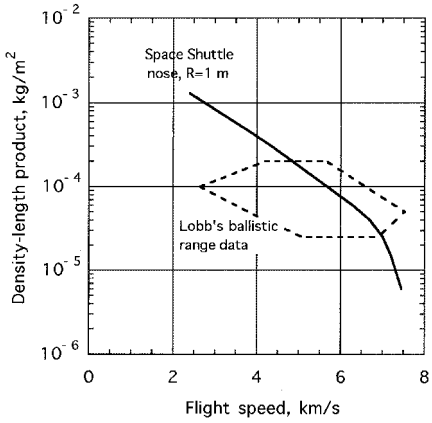

Fig. 4 Density-length product values covered by Lobb's experiment[13] compared with Space Shuttle values.

There exist in the literature several schlieren photographs of the shock-layer flow over a sphere in the equilibrium region, from which the correct values of shock standoff distance can be determined (see, e.g., Ref. 12). The standoff distance values in the nonequilibrium-flow regime, which are more difficult to obtain because of the low density involved, were obtained by Lobb.[13] The data are reproduced in Fig. 3, and are compared with similar data taken in an expansion tube.[14] The figure shows that measured shock standoff distances are substantially larger than the equilibrium values in the nonequilibrium range, as expected.

The range of density-length product values covered by Lobb's data set[13] is shown in Fig. 4. The figure shows that the tested range overlaps with that of the Space Shuttle nose region in the high-speed range. This means that the flow over most of the Space Shuttle vehicle will be in nonequilibrium for the high-speed range. For the low-speed range, the density–length product is larger in flight than the values produced in the ballistic range test, implying that equilibrium will prevail there.

In addition to the sphere tested by Lobb,[13] blunted cones and cones with flares could be flown and their flowfield visualized in a ballistic range. From their schlieren and thermographic photographs, shock shapes, boundary-layer transition points,[12] and structures of separated flows, shock-/boundary-layer-interaction flows, and leeward-side/base flows could be made visible.

Pitot and Heat Transfer Measurements

The basic characterization measurements in a wind tunnel consist of radial surveys of pitot total pressures and heat transfer rates to the stagnation point of a sphere. The pitot total pressure is governed only by the momentum equation in the axial direction, and so its ratio to the reservoir pressure is a function only of the effective nozzle area ratio independently of any chemical reactions occurring within the inviscid core of the nozzle. Since flow reaches equilibrium at the edge of the boundary layer over the tested model in most cases, the stagnation-point heat transfer rate is independent of the chemical state of the freestream flow.

The effective area ratio that determines the pitot pressure is determined by the displacement thickness of the boundary layer growing over the nozzle wall δ. To understand the real-gas effects on δ, one tacitly assumes that the static pressure is constant across the boundary layer. Then, because the equation of state in a dissociated gas is $p = \rho RTZ$, there follows:

$$\delta = \int_0^\infty \left(1 - \frac{\rho U}{\rho_e U_e}\right) \mathrm{d}y \approx \int_0^\infty \left(1 - \frac{T_e Z_e U}{TZU_e}\right) \mathrm{d}y$$

where the subscript e signifies the edge of boundary layer. In a real-gas wind tunnel, both the temperature ratio T/T_e and the

compressibility ratio Z/Z_e are smaller than in a perfect gas. As a result, the δ value is smaller.

In an extreme case of very large T_eZ_e and very small T_wZ_w, δ could even be negative. Such a phenomenon would resemble a flow of steam passing through a cold pipe. Because of condensation of the vapor into liquid at and near the wall in this case, the Z value shrinks from unity at the edge to zero at the wall, and the displacement thickness becomes negative as a result.

To theoretically calculate the displacement thickness of the boundary layer growing over the nozzle wall, one must know the interaction of chemical reactions with the turbulent boundary layer growing over the wall. The chemical reactions in the cold region of the boundary layer are the same as those occurring in an expanding nozzle flow.[15] As will be shown, the chemical reactions in an expanding flow are not well known. Therefore, it is unrealistic to expect to calculate with confidence the displacement thickness over the nozzle wall in a real-gas regime. Conversely, the effective area ratio of a nozzle, or the resulting pitot total pressure, cannot be used as an indicator of the chemical state of the inviscid flow in a real-gas tunnel.

Chemical Reactions in Nozzle

To determine the chemical state of the gas in the test section of an impulse tunnel, the concentrations of chemical species and vibrational temperatures must be measured. The commonly used method for concentration measurement is mass-spectrometry,[16–18] although an optical spectroscopic technique is being developed.[19] Spectroscopic methods are used in measuring the vibrational temperature.[20]

Vibrational temperatures and species mole fractions at the nozzle exit have been measured for an arc-heated facility in Refs. 16 and 20. There are presently many computer codes for the calculation of the chemical reactions occurring in a hypersonic nozzle. Most codes use the conventional so-called one-temperature model such as that used in the NENZF code.[21] References 22 and 23 show that the calculated vibrational temperatures generally agree with the measured values, but that the conventional theoretical model gives species concentration values that are greatly different from the measured values. The discrepancies are as follows:

1) The measured oxygen atom concentrations are substantially lower than the calculated values.

2) The measured nitrogen atom concentrations are many orders of magnitude greater than the calculated values.

3) The measured nitric oxide concentrations are substantially higher than the calculated values.

A multitemperature reaction model was introduced in Ref. 22 to explain the measured data. The model is based on the assumption that nozzle flows contain a significant concentration of electronically excited oxygen atoms, and that the endothermic Zeldovich reactions occur faster because of their presence. The model produces a result that is closer to the measured data, but fails to bring about a complete agreement.

Recently, similar measurements of species concentration have been made in a shock tunnel.[17,18] The measurements were made at a reservoir pressure of 14 MPa over an enthalpy range from 5.6 to 21 MJ/kg. The authors caution that the data values may not be accurate at enthalpies above 15 MJ/kg because of possible mixing of the driver gas with the driven gas. The measured data were compared with the values calculated by the NENZF code. A discrepancy was found between the measured and the calculated values. The discrepancy is qualitatively the same as that found for the arcjet flow, but its extent was larger.

Calculations are performed in this work for these shock-tunnel test conditions first using the conventional one-temperature model. The conventional reaction rate coefficient values given in Ref. 24 were used. The species concentrations resulting from the calculations are shown in Figs. 5a–5e, marked

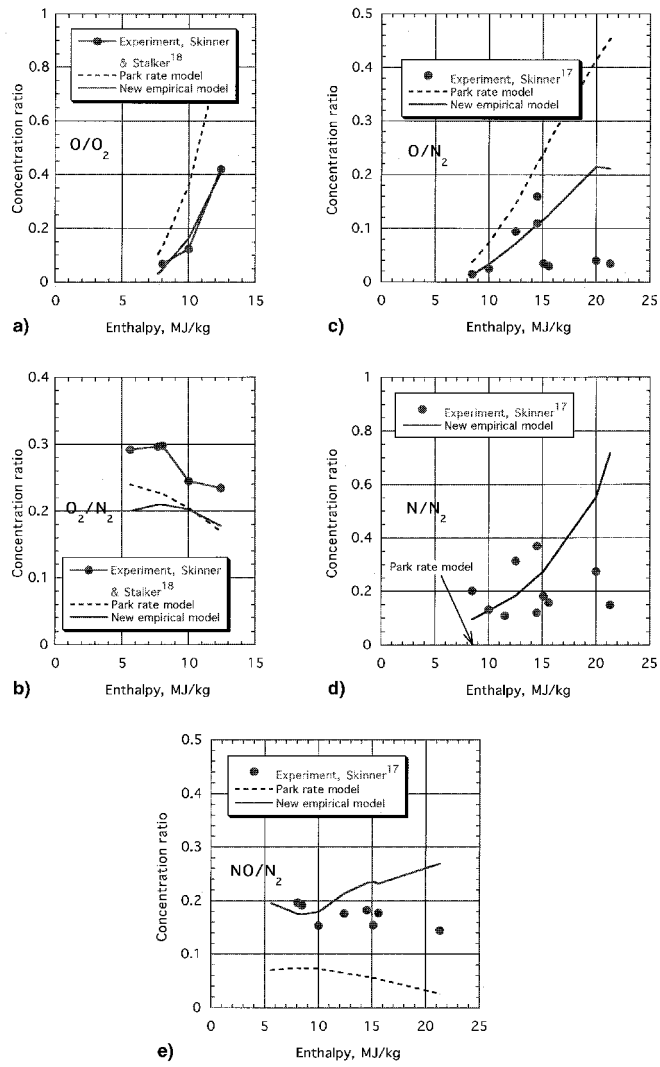

Fig. 5 Comparison between the measured and calculated species concentration ratios for the experiment of Skinner[17] and Skinner and Stalker[18]: a) O/O_2, b) O_2/N_2, c) O/N_2, d) N/N_2, and e) NO/N_2.

Park rate model, and are compared with the experimental data. The calculated values differ greatly from the measured values, especially on the nitrogen atom concentrations. The calculated values are slightly closer to the measured values than those obtained using the NENZF rate coefficients.[17]

To fit the experimental data, a new empirical model is proposed in this work. The model assumes the following:

1) The forward reaction of the first Zeldovich reaction, $O + N_2 \rightarrow NO + N$, occurs with the activation temperature of 38,400 K reduced by $\Delta E = 32{,}000 + 4 \times 10^6/T$ K.

2) The forward reaction of the second Zeldovich reaction, $O + NO \rightarrow O_2 + N$, occurs with a zero activation temperature.

3) The rate coefficients for three-body recombination of nitrogen, $N + N + M \rightarrow N_2 + M$, is 10^{-3} times the values in Ref. 24 for all third-body types M.

4) The rate coefficients for three-body recombination of oxygen, $O + O + M \rightarrow O_2 + M$, is 10^{-6} times the values in Ref. 24 for all third-body types M.

Assumptions 1 and 2 are the same in principle as those made in Ref. 22 and express the hypothesis that many oxygen atoms exist in their electronically excited (^1D and ^1S) states, and that the endothermic Zeldovich reactions are fast for these atoms. How the populations of these electronically excited states are maintained at a high level is not known exactly. However, a clue can be found in the experiment reported in Ref. 25. In that experiment, in an expanding flow of pure nitrogen, a large

concentration of N_2 molecules excited to high electronic states, $B^3\Pi_g$ and $C^3\Pi_u$, were found early in the cooling process. However, when oxygen was added to the flow, these excited N_2 molecules disappeared. This implies that the electronic energy of those excited N_2 molecules are transferred to O or O_2. Inevitably, one of its consequences is to produce electronically excited O atoms.

The electronically excited $N_2(B)$ and $N_2(C)$ can be produced by a process known as inverse-predissociation, $N + N \rightarrow N_2(B,C)$. This process is a binary process and can occur at a significant rate, even at low densities. Although spectroscopically invisible, the same process is expected to occur to all states in the neighborhood of the B and C states. Those excited N_2 states can be produced also via three-body recombination processes. The total multiplicity of all known electronic states of N_2 in the neighborhood of the B and C states is 40 times that of the X state. According to the principle of chemical reactions, this means that the rates of three-body recombination into those states could be 40 times that into the X state in an expanding flow. Since these energy levels are high, they can also dissociate back into N + N at relatively low temperatures.

The phenomenon assumed in 3 may occur as a result of the electron-impact dissociation of N_2. It is known that electrons are 1000 times more efficient than heavy particles as a third body in dissociating N_2.[26] Electrons exist in impulse facilities in a greater concentration than calculated because of the impurities. These electrons are likely to be hotter than the heavy particles because of the preferential heating phenomenon.[27] As a result, at the point of freezing of nitrogen recombination, the concentration of N atoms is likely to be that corresponding to the equilibrium value corresponding to the local electron temperature.

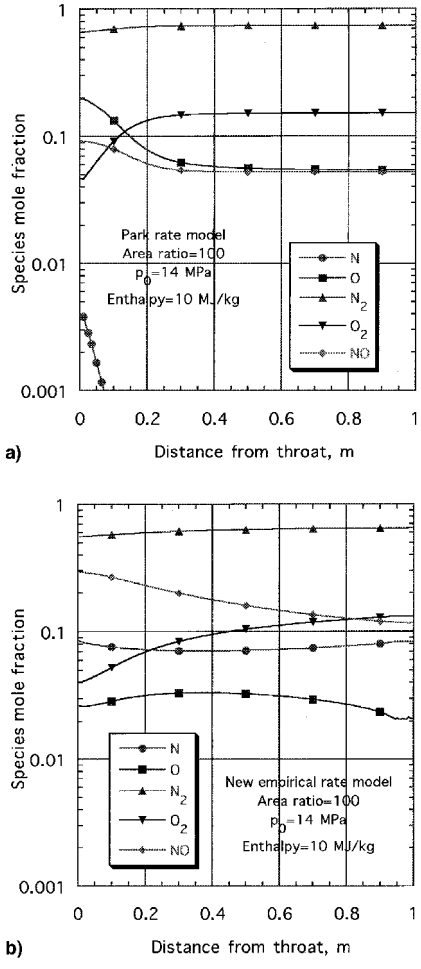

Fig. 6 Axial variation of species mole fractions for the experimental case of Ref. 17: a) Park rate model[24] and b) new empirical model.

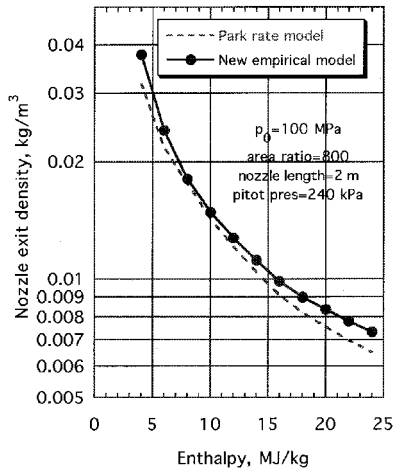

Fig. 7 Nozzle exit densities in the experiments of Refs. 17 and 18 calculated by two rate models.

The phenomenon assumed in 4 may also be a result of the existence of a large concentration of electronically excited N_2 molecules. For instance, a $N_2(C)$ could dissociate O_2 via $N_2(C) + O_2(X) \rightarrow N_2(A) + O + O$. The $N_2(A)$ so formed can be collisionally dissociated even at relatively low temperatures.

In Figs. 5a–5e, the concentration values calculated using the new empirical model are compared with the experimental data. The calculations were started in the subsonic region upstream of the throat. As seen in the figures, the new model gives a fairly close agreement with the experimental data below 15 MJ/kg, where the experimental data are believed to be accurate.

The calculated variation of species mole fractions in the axial direction in the nozzle is shown in Figs. 6a and 6b for the two rate models for an enthalpy of 10 MJ/kg. As seen in these figures, there is a considerable difference in the calculated species concentrations between the two cases. The difference starts from the subsonic region.

The calculated density at the nozzle exit is shown for the two cases in Fig. 7. The new rate model gives discernibly higher density values than the conventional model. This is because a less amount of chemical energy is transferred into the translational mode in the empirical model, and, therefore, produces lower temperatures. Though not shown, the pitot total pressures for the two cases are nearly identical, underscoring the argument given in the Facility Limitations section that pitot pressure is independent of chemical phenomena.

Density Ratios Across Shock

The electronically excited O atoms, N_2 molecules, and both unexcited and excited N atoms are all highly chemically active. The chemical reactions behind a shock wave formed over a model placed in the test section of an impulse tunnel will become faster than in undisturbed air because of their presence in the freestream. The impurity species may also be chemically active. However, unless their mole concentration is in the same order as those of the major species, their presence should not affect the flow significantly. The enhancement of Damköhler number has already been observed experimentally in an arcjet flow,[9] as mentioned in the Facility Limitations section. The average density ratio between the shock layer over a blunt body and the freestream will then be affected by the enhancement phenomenon, except when the shock-layer flow is unconditionally in an equilibrium regime. The shock standoff distance for a blunt body will be affected accordingly in the nonequilibrium regime.

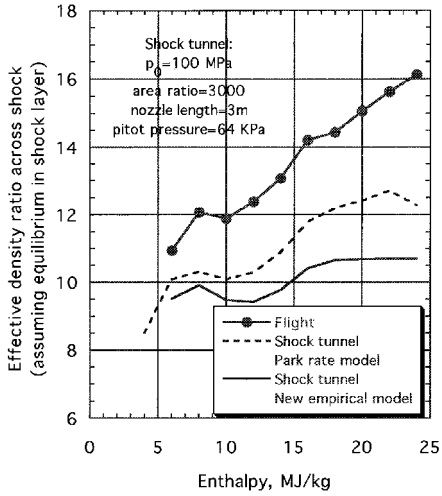

Fig. 8 Calculated density ratios across a normal shock wave compared with the flight values.

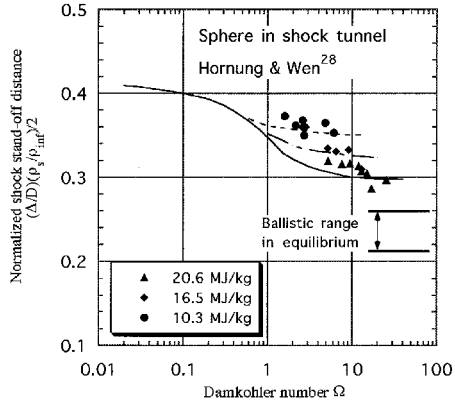

Fig. 9 Normalized shock standoff distance for sphere in a shock tunnel.[28]

The average density ratio was calculated in the present work for a shock layer over a model placed in a shock tunnel using both the conventional rate model and the new empirical model. For this purpose, the shock-layer pressure and enthalpy were first determined using the hypersonic approximation, $p_t = \rho_\infty U_\infty^2$, $H = U_\infty^2/2$, and the resulting equilibrium density was taken to be the average shock-layer density. The approximation overestimates the density ratio slightly. The reservoir pressure was taken to be 100 MPa, and the nozzle area ratio and length were assumed to be 3000 and 3 m, respectively. The results are shown in Fig. 8 and are compared with the values expected in flight.

As seen in the figure, the density ratio is smaller in a shock tunnel than in flight. The new empirical rate model gives smaller density ratios than the conventional model. This implies that the shock standoff distances in a shock tunnel will be larger than in flight.

According to Fig. 8, the density ratio value obtainable in a shock tunnel is the closest to the flight value at an enthalpy of 8 MJ/kg. Thus, the degree of simulation is the best at this enthalpy. Also, the difference in the density ratio values predicted by the two reaction rate models is the smallest at this enthalpy, implying that any theoretical corrections made to the experimental data will be most reliable at that enthalpy. The density ratio reaches a constant value at around 18 MJ/kg, which implies that, for the purpose of simulating the real-gas effects, it is needless to operate at higher enthalpies. The density ratio at 18 MJ/kg is only slightly larger than that at 8 MJ/kg. Because the density ratio values in a perfect gas, in the tunnel flow, and in flight are 6, 10, and 12 at 8 MJ/kg, respectively, one may say that two-thirds of the real-gas effects is realized in the tunnel at that enthalpy. In comparison, at an enthalpy of 20 MJ/kg, the test realizes only one-half of the true real-gas effects.

Shock Standoff Distance in Shock Tunnel

The shock standoff distances for spheres and cylinders have been measured in a shock tunnel by Hornung and Wen[28] for various gases. For nitrogen and carbon dioxide, the shock standoff distance was found to decrease significantly as the Damköhler number was increased. At low Damköhler numbers, the standoff distance was that corresponding to the perfect gas, and at high Damköhler numbers, it was that of an equilibrium flow. The observed behavior agreed closely with the calculations.

However, for airflows, the changes in shock standoff distance caused by the changes in the Damköhler number were not large.[28] In Fig. 9, the shock standoff distance data for air are reproduced. In the figure, the abscissa Ω is a special Damköhler number defined in Ref. 28. The quantities ρ_{inf} and ρ_s are the density of the freestream and immediately behind the normal shock wave, and Δ and D are shock standoff distance and body diameter, respectively. The quantities Ω, ρ_{inf}, and ρ_s were calculated in Ref. 28 using a conventional model that is not compatible with the experimental data of Refs. 17 and 18. Therefore, accuracy of these quantities is in doubt.

However, the main features of the experimental data can be appreciated. According to the data, the measured shock standoff distance in an airflow decreases only slightly as the flow Damköhler number is increased. From the schlieren photographs obtained in ballistic ranges and from calculations, the shock standoff distance for the equilibrium flow is known. They are shown in Fig. 9 and are compared with the shock-tunnel data. The difference between the two sets of data is apparent. The extent of the reduction in shock standoff distance caused by chemical reactions obtained in the shock-tunnel test is only about one-half, or less than that obtained in ballistic range tests. The extent of the standoff distance reduction at 10 MJ/kg is less than predicted in Fig. 8. This could be because of the following:

1) The experiment was conducted at reservoir pressures less and nozzle lengths shorter than those assumed in Fig. 8.

2) The quantities Ω, ρ_{inf}, and ρ_s were calculated erroneously.

Qualitatively, Fig. 9 is in agreement with Fig. 8, in that only part of the true extent of the real-gas effects is realized in an impulse tunnel.

Test Strategy

One can now formulate the best strategy for the simulation of real-gas effects in an impulse tunnel. As a prerequisite, a meaningful test can be conducted only in a large facility and only at a reservoir pressure of the order of 100 MPa. The density–length product in the flight condition to be simulated is first determined. Then, from the ballistic range data, one determines the in-flight shock standoff distances and shock-layer thicknesses for spheres and cones, the boundary-layer transition point for a cone of choice, and the separated-flow parameters for a flared-cone for that density-length product value. The tunnel is operated with those spheres and cones to determine the equivalent density-length product value that gives similar shock-layer thicknesses, transition points, and separated-flow parameters as in flight, allowing for the intrinsic differences described earlier. That is, the effective Reynolds and Damköhler numbers for the tunnel are determined. The needed tests of the real-gas effect phenomena are carried out at these effective Reynolds and Damköhler numbers. According to the foregoing arguments, the shock-layer thicknesses observed in the tunnel should be closer to the flight values than to the perfect-gas values.

For comparison purposes, one may conduct the same experiment in a perfect gas regime. This can be achieved by

Table 1 Calculated flow conditions for real-gas simulation

Test condition	Tunnel	Tunnel	Flight
Body length, m	1	1	30
Gas	Air	N_2	Air
Enthalpy, MJ/kg	8	3	8
Reservoir pressure, MPa	100	1.37	
Nozzle exit conditions			
Area ratio	3000	100	
Pressure, Pa	1205	663	1380
Temperature, K	811	299	210
Density, kg/m^3	4.82^{-3}	7.47^{-3}	2.09^{-4}
Velocity, m/s	3632	2320	4000
O mole fraction	1.93^{-4}	0	0
N mole fraction	1.90^{-3}	0	0
NO mole fraction	1.26^{-1}	0	0
Effective Mach number	≈6.5	6.58	14
Reynolds number	10^6	10^6	10^6
Equilibrium condition behind normal shock			
Pressure, Pa	6.36^4	4.02^4	3.34^3
Temperature, K	3982	2529	3978
Density, kg/m^3	4.78^{-2}	5.35^{-2}	2.67^{-3}
O mole fraction	2.73^{-1}	5.01^{-5}	3.25^{-1}
N mole fraction	1.68^{-3}	6.03^{-7}	2.13^{-3}
NO mole fraction	3.68^{-2}	1.18^{-4}	1.52^{-2}
Density ratio across shock	10.2	7.16	12.8
Simulating altitude, km			63

operating the facility with nitrogen at an enthalpy of 3 MJ/kg or lower. The operating conditions must be adjusted to reproduce the Mach number and Reynolds number of the real-gas test. The results of this test are compared with those of the real-gas test. The difference between the two should be judged to be the real-gas effects. For a crude approximation, at 8 MJ/kg, the magnitude of the real-gas effects so deduced can be multiplied by 1.5 to account for the fact that the facility simulates only two-thirds of the true extent of the real-gas effects. For test results obtained at higher enthalpies, a higher factor must be multiplied. More precise corrections should be made by utilizing numerical computations.

The typical operating conditions of an impulse tunnel for such a test are compared with the corresponding flight conditions in Table 1. The real-gas tunnel conditions are calculated using the new empirical model. The effective Mach number shown in the table is an average between the equilibrium and the frozen Mach numbers. The table shows that, even with an area ratio of 3000, the nozzle exit Mach number in a real-gas flow is only 6.5. The reference nitrogen test is designed to reproduce the Mach number and the Reynolds number of the real-gas test.

The presence of metallic impurities in the tunnel is automatically accounted for in this validation procedure. As long as the in-flight flow phenomena such as shock shapes and transition points are correctly reproduced, the fact that the test gas contains a small amount of metallic impurities should not matter.

The present reasoning points to the need for more measurements in ballistic ranges, more accurate direct measurements of chemical compositions in the flow produced by an impulse tunnel, and theoretical works to interpret the test results. A balance should be maintained between the impulse-tunnel and ballistic-range tests, and between experiments and theoretical efforts for a meaningful utilization of impulse tunnels.

Conclusions

Real-gas impulse tunnels are expected to be useful in simulating four, or possibly five, types of real-gas problems. The chemical state of the airflows in such a tunnel cannot be described by the conventional reaction rate model, but can be with a new empirical model that assumes fast Zeldovich reactions of the excited oxygen atoms and slow three-body recombination reactions. When a tunnel is operated at an enthalpy of 8 MJ/kg, the density ratios and the shock standoff distances are likely to be the closest to those in flight, and about two-thirds of the real-gas effects in flight could be simulated in the tunnel at that enthalpy. The impulse tunnel tests are valid when they are conducted at the effective Reynolds and Damköhler numbers that produce similar shock shapes and transition points as those obtained in the ballistic range experiments for simple geometries.

Acknowledgments

The author wishes to express sincere thanks to NASA Ames Research Center for permission to use the information obtained there, and to the staff of the Shock Tunnel Group for providing the information.

References

[1]Park, C., "Laboratory Simulation of Aerothermodynamic Phenomena: A Review," AIAA Paper 92-4025, June 1992.

[2]Crowder, R. S., and Moote, J. D., "Apollo Entry Aerodynamics," *Journal of Spacecraft and Rockets*, Vol. 6, No. 3, 1969, pp. 302–307.

[3]Romere, P. O., and Whitnah, A. M., "Space Shuttle Entry Longitudinal Aerodynamic Comparisons of Flights 1-4 with Preflight Predictions," *Shuttle Performance: Lessons Learned*, compiled by J. P. Arrington and J. J. Jones, NASA CP-2283, 1983, pp. 283–307.

[4]Weilmuenster, K. J., Gnoffo, P. A., and Greene, F. A., "Navier-Stokes Simulation of the Orbiter Aerodynamic Characteristics Including Pitch Trim and Body Flap," *Journal of Spacecraft and Rockets*, Vol. 31, No. 3, 1994, pp. 355–366.

[5]Goodrich, W. D., Derry, S. M., and Bertin, J. J., "Shuttle Orbiter Boundary-Layer Transition—A Comparison of Flight and Wind Tunnel Data," AIAA Paper 83-0485, Jan. 1983.

[6]Cavolowsky, J. A., "Flow Characterization in Shock Tunnels," Lecture Notes, AIAA Short Course on Aerothermodynamic Facilities and Measurement, June 1994.

[7]Davies, C. B., and Park, C., "Trajectories of Solid Particles Spalled from a Carbonaceous Heat Shield," *Entry Heating and Thermal Protection System: Space Shuttle, Solar Starprobe, Jupiter Galileo Probe*, edited by P. E. Bauer and H. E. Collicott, Vol. 85, Progress in Astronautics and Aeronautics, AIAA, New York, 1983, pp. 472–495.

[8]Schneider, K. P., and Park, C., "Shock Tube Study of Ionization Rates of NaCl-Contaminated Argon," *Physics of Fluids*, Vol. 18, No. 8, 1975, pp. 969–981.

[9]Babikian, D. S., Gopaul, N. K. J. M., and Park, C., "Measurement and Analysis of Nitric Oxide Radiation in an Arcjet Flow," *Journal of Thermophysics and Heat Transfer*, Vol. 8, No. 4, 1994, pp. 737–743.

[10]Cable, A. J., "Upgrade of Ballistic Range Facilities at AEDC—Two-Thirds Complete," AIAA Paper 93-0349, Jan. 1993.

[11]Anderson, J. D., *Hypersonic and High Temperature Gas Dynamics*, McGraw–Hill, New York, 1989, p. 274.

[12]Reda, D. C., "Comparative Transition Performance of Several Nosetip Materials as Defined by Ballistic Testing," *ISA Transactions*, Vol. 19, No. 1, 1979, pp. 83–98.

[13]Lobb, R. K., "Experimental Measurement of Shock Detachment Distance on Spheres Fired in Air at Hypervelocities," *The High Temperature Aspects of Hypersonic Flow*, edited by W. C. Nelson, Pergamon, New York, 1964, pp. 519–527.

[14]Miller, C. G., "Shock Shapes on Blunt Bodies in Hypersonic-Hypervelocity Helium, Air, and CO_2 Gas Flows, and Calibration Results in Langley 6-Inch Expansion Tube," NASA TN D-7800, Feb. 1975.

[15]Armenise, I., Capitelli, M., Colonna, G., and Gorse, C., "Nonequilibrium Vibrational Kinetics in the Boundary Layer of Re-Entering Bodies," *Journal of Thermophysics and Heat Transfer*, Vol. 10, No. 3, 1996, pp. 397–405.

[16]MacDermott, W. N., and Dix, R. E., "Mass Spectrometric Analysis of Nonequilibrium Airflows," *AIAA Journal*, Vol. 10, No. 4, 1972, pp. 494–498.

[17]Skinner, K. A., "Mass Spectrometry in Shock Tunnel Experiments of Hypersonic Combustion," Ph.D. Dissertation, Univ. of Queensland, Australia, March 1994.

[18]Skinner, K. A., and Stalker, R. J., "Mass Spectrometer Measurements of Test Gas Composition in Shock Tunnel," *AIAA Journal*, Vol. 34, No. 1, 1996, pp. 203–205.

[19]Meyer, S. A., Sharma, S. P., Bershader, D., Whiting, E. E., Ex-

berger, R. J., and Gilmore, J. O., "Absorption Line Shape Measurement of Atomic Oxygen at 130 nm Using a Raman-Shifted Excimer Laser," AIAA Paper 95-0290, Jan. 1995.

[20]MacDermott, W. N., and Marshall, J. G., "Nonequilibrium Nozzle Expansion of Partially Dissociated Air: A Comparison of Theory and Electron-Beam Experiment," Arnold Engineering and Development Center, TR-69-66, July 1969.

[21]Lordi, J. A., Mates, R. E., and Moselle, J. R., "Computer Program for the Numerical Solution of Nonequilibrium Expansions of Reacting Gas Mixtures," NASA CR-472, May 1979.

[22]Park, C., and Lee, S. H., "Validation of MultiTemperature Nozzle Flow Code," *Journal of Thermophysics and Heat Transfer*, Vol. 9, No. 1, 1995, pp. 9–16.

[23]Park, C., "Estimation of Excitation Energy of Diatomic Molecules in Expanding Nonequilibrium Flows," *Journal of Thermophysics and Heat Transfer*, Vol. 9, No. 1, 1995, pp. 17–25.

[24]Park, C., "Assessment of Two-Temperature Kinetic Model for Ionizing Air," *Journal of Thermophysics and Heat Transfer*, Vol. 3, No. 3, 1989, pp. 233–244.

[25]Laux, C. O., Gessman, R. J., and Kruger, C. H., "Mechanism of Ionization Nonequilibrium in Air and Nitrogen Plasmas," AIAA Paper 95-1989, June 1995.

[26]Sharma, S. P., Gillespie, W. D., and Meyer, S. A., "Shock Front Radiation Measurement in Air," AIAA Paper 91-0573, Jan. 1991.

[27]Park, C., *Nonequilibrium Hypersonic Aerothermodynamics*, Wiley, New York, 1990, Chap. 4.

[28]Hornung, H. G., and Wen, C. Y., "Nonequilibrium Dissociating Flow over Spheres," AIAA Paper 95-0091, Jan. 1995.